Dense Attosecond Electron Sheets from Laser Wakefields Using an Up-Ramp Density Transition

F. Y. Li,[1] Z. M. Sheng,[1,2,*] Y. Liu,[1] J. Meyer-ter-Vehn,[3] W. B. Mori,[4] W. Lu,[5] and J. Zhang[1,2]

[1]*Key Laboratory for Laser Plasmas (MoE) and Department of Physics, Shanghai Jiao Tong University, Shanghai 200240, China*
[2]*Beijing National Laboratory for Condensed Matter Physics, Institute of Physics, CAS, Beijing 100190, China*
[3]*Max-Planck-Institut für Quantenoptik, D-85748 Garching, Germany*
[4]*Department of Physics and Astronomy and Department of Electrical Engineering,
University of California, Los Angeles, California 90095-1547, USA*
[5]*Department of Engineering Physics, Tsinghua University, Beijing 100084, China*

Controlled electron injection into a laser-driven wakefield at a well defined space and time is reported based on particle-in-cell simulations. Key novel ingredients are an underdense plasma target with an up-ramp density profile followed by a plateau and a fairly large laser focus diameter that leads to an essentially one-dimensional (1D) regime of laser wakefield, which is different from the bubble (complete blowout) regime occurring for tightly focused drive beams. The up-ramp profile causes 1D wave breaking to occur sharply at the up-ramp-plateau transition. As a result, it generates an ultrathin (few nanometer, corresponding to attosecond duration), strongly overdense relativistic electron sheet that is injected and accelerated in the wakefield. A peaked electron energy spectrum and high charge ($\sim$ nC) distinguish the final sheet.

PACS numbers: 52.38.Kd, 52.59.−f

Ultrashort electron bunches are of key importance for future ultrafast science, either in probing ultrafast processes or for driving ultrashort radiations. High-power lasers make it possible to generate such electron bunches via laser-plasma interactions [1]. It has been demonstrated that laser wakefield accelerators can generate femtosecond bunches with a few percent of the energy spread [2,3]. However, producing dense electron bunches with attosecond duration and even small absolute energy spread, for advanced applications such as coherent x-ray generation [4], remains a challenge. To produce attosecond bunches, a number of schemes has been proposed, using direct laser interactions such as vacuum acceleration by tailored laser pulses [5], laser-illuminated ultrathin plasma layers [6], overdense plasma boundaries [7] or droplets [8], and stochastic slicing of electron pulses [9]. However, these schemes generally require challenging technologies, namely, fine control on laser-target profiles and an ultrahigh contrast ratio of lasers.

On the other hand, the density singularities that arise in nonlinear plasma waves are very thin, so that, if the breaking of the wave can be controlled to occur in a limited space and time, they could be the source of attosecond bunches with monochromatic spectra [10]. These density spikes have been proposed to be used as flying mirrors for light Doppler upshift [11]. However, thermal effects [12] may limit the wave amplitude well below the cold wave breaking limit. Also, other ways have been proposed by injecting plasma electrons into the accelerating wave in a controlled manner such as using colliding pulses [13], higher-order ionizations [14], down-ramp density transitions [15], and magnetic fields [16]. Still, the generated bunches often have femtosecond duration, pC charge, and an energy spread exceeding a few percent.

In this Letter, we report a new method of controlled injection that is able to generate dense attosecond electron sheets (AESs) in laser wakefields. The idea is to send an intense laser with a fairly broad spot through an underdense plasma slab with an up-ramp density profile followed by a plateau. The phase velocity of the wakefield switches suddenly from above to below the light speed c at the up-ramp-plateau transition (UPT), where 1D wave breaking occurs sharply. The density spike characteristic for wave breaking is then trapped in the first wave bucket and gets accelerated as a whole without much broadening. The present method requires laser powers of some 100 TW at intensities in the order of 10^{19} W/cm^2.

Figure 1(a) shows the present scheme. As first pointed out by Katsouleas [17], the phase velocity of a wake driven by a particle beam moving with constant velocity in a density gradient will change due to the density dependence of the wavelength. This is referred to as the accordion effect, and the modification becomes stronger for each successive bucket. For a laser pulse, this phenomenon is more complicated since the laser group velocity also depends on density. In 1D laser wakefields, the normalized phase velocity for each bucket (Nth) is $\beta_{\mathrm{ph}}(x) = \beta_{\mathrm{gr}}(x)/(1 + N d\lambda_p/dx)$, where β_{gr} and λ_p are the normalized laser's group velocity and the wake's wavelength, respectively, and both may depend nonlinearly on laser amplitude a_0. In the linear regime $a_0 \ll 1$, β_{ph} reduces to

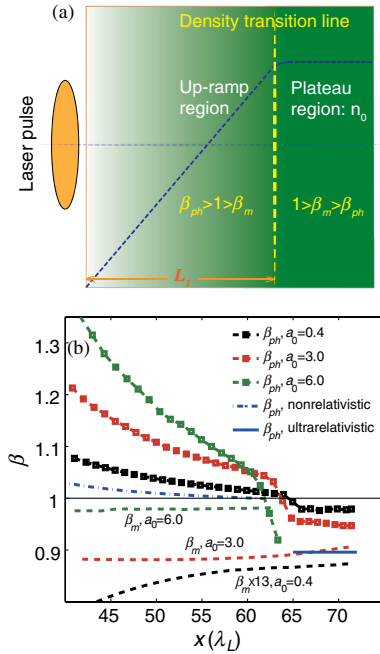$$\beta_{\mathrm{ph}}(x) = \frac{1 - \omega_p^2/2\omega_L^2}{1 - (|\xi|/2\omega_p^2)(d\omega_p^2/dx)}, \qquad (1)$$

FIG. 1 (color online). (a) Schematic of AES generation. Localized electron injection occurs as $\beta_{\rm ph}$, at which the apex of the first wakefield bucket is moving, undergoes a fast switch from above to well below unity near the UPT. (b) Evolution of $\beta_{\rm ph}$ and β_m from 1D PIC simulations, where the initial plasma density rises linearly from zero at $x = 20\lambda_L$ to $0.04n_c$ at $65\lambda_L$ and then keeps constant.

where x is the propagation direction, ω_p is the plasma frequency, ω_L is the laser frequency, and $-\xi = \beta_{\rm gr}ct - x$ denotes the distance from the local position x to the drive laser. For a down-ramp profile $dn/dx < 0$, Eq. (1) indicates that $\beta_{\rm ph} < \beta_{\rm gr} < 1$ and $\beta_{\rm ph}$ falls further as the laser propagates. Here, $n = \omega_p^2/\omega_L^2$ is the plasma density. This slowing down of wake due to the accordion effect is the basis of density-gradient injection [15]. In contrast, for an up-ramp profile $dn/dx > 0$, Eq. (1) indicates that $\beta_{\rm ph}$ can exceed unity and asymptotes to $\beta_{\rm gr}(x)$ along the up ramp, as shown in Fig. 1(b). One finds $\beta_{\rm ph} > 1$ because the plasma wavelength ($\lambda_p \propto n^{-1/2}$) is shrinking more rapidly than $\beta_{\rm gr}$ is decreasing. On the other hand, when the first bucket reaches the plateau region, $\beta_{\rm ph}$ reduces to $\beta_{\rm gr}$, which is less than unity. For $a_0 < 1$, such a fast switch of $\beta_{\rm ph}$ from above to below unity actually does not lead to electron injection because the wave amplitude is sufficiently small so that the maximum electron fluid velocity $v_m = c\beta_m \propto a_0^2$ is still far below c. A weakly relativistic case ($a_0 = 0.4$) is presented in Fig. 1(b).

The situation differs significantly at relativistic intensity $a_0 > 1$. As shown in Fig. 1(b) by the square-dashed curves, the superluminality of $\beta_{\rm ph}$ along the up ramp is enhanced because of the nonlinear increase of λ_p. Therefore, the up ramp prevents premature wave breaking, even though β_m is now highly relativistic, as shown in Fig. 1(b). Meanwhile, as

the laser approaches the plateau, $\beta_{\rm ph}$ decreases gradually so that the difference between $\beta_{\rm ph}$ and β_m reduces. Following the continuity equation [10], the density wake induced along the ramp, approximated by $n_w = n\beta_{\rm ph}/(\beta_{\rm ph} - \beta_e)$, will develop into an ultrashort overdense spike comprising most of the energetic forward-going electrons located near the spike center. Here, β_e is the normalized electron fluid velocity. In addition, the phase velocity of the nonlinear wake in the plateau $\beta_{\rm ph}^{\rm plat}$ is well below the linear group velocity of the laser pulse, owing to complex nonlinear effects [18,19]. At $a_0 = 6$, one finds that $\beta_{\rm ph}^{\rm plat}$ almost reduces to the 1D ultrarelativistic limit [19] $\beta_{\rm ph}^{\rm lim} \simeq (1 - 5\omega_{p0}^2/\omega_L^2)^{1/2}$ with $\omega_{p0} \propto n_0^{1/2}$. As a result, $\beta_e > \beta_{\rm ph}^{\rm plat}$ suddenly occurs near the UPT. This allows a well defined group of electrons within the highly converged spike to get trapped near the same value of x. It is these trapped electrons which form a dense AES.

To verify this process, we first performed 1D particle-in-cell (PIC) simulations using the KLAP code [20]. The simulation profile is identical with Fig. 1. A linearly polarized laser pulse with normalized vector potential $a = a_0\sin^2(\pi t/\tau_L)$ initially impinges on the tailored plasma slab with plateau density of $n_0 = 0.04n_c$, where $a_0 = 6$ corresponds to a peak intensity of 4.9×10^{19} W/cm^2, $\tau_L = 10T_L$, and $n_c = 1.1 \times 10^{21}$ cm^{-3} is the critical density for $\lambda_L = 1$ μm. A grid size of $0.001\lambda_L$ is used to resolve the fine structure of AES. To avoid possible effects from a sharp vacuum-plasma interface [21], the ramp length L_1 is set to be $45\lambda_L$, which is much larger than a plasma skin depth c/ω_{p0}. Such a hundred-micron ramped plasma is now available with several techniques, such as the laser machining of gas jets [22]. In addition, the plasma should have a small longitudinal temperature, i.e., $T_\parallel^e \lesssim 10$ eV, while the transverse temperature $T_\perp^e$ is of less importance.

The spatial-temporal evolution of the electron density is shown in Fig. 2(a). Consistent with the above analysis, $\beta_{\rm ph}$ is superluminal and asymptotes to unity along the up ramp. The width of the density wave crest given by $\delta d \propto (\beta_{\rm ph} - \beta_m)^{3/2}$ gradually shrinks as $\beta_{\rm ph}$ approaches β_m [15] and finally evolves into an overdense spike. This process continues up to the UPT, where the spike starts to be trapped in the first wave bucket. The first density wave crest is presented at five distinct times in Fig. 2(b). After the transition, a strongly overdense electron bunch of about ten attosecond duration (the AES) is obtained. We incorporate particle tracking into the following to investigate in more detail. Figure 2(c) presents the temporal evolution of two AES electrons obtained for two different n_0. It is seen that both electrons start responding to the laser field at $t = 67T_L$ and get trapped after a single plasma period. It verifies that there is no wave breaking along the up ramp and that it is the UPT that causes the localized injection.
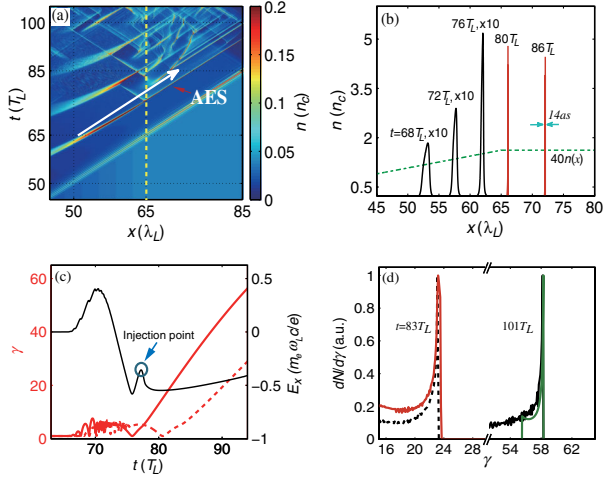
FIG. 2 (color online). Results of 1D PIC simulation. (a) Spatial-temporal plot of the electron density. The dashed line marks the UPT at $x = 65\lambda_L$, and the white arrow is parallel to $x = t$. (b) The first density wave crest before (black curve) and after (red curve) the transition. The dashed line shows the initial target profile. (c) Temporal evolution of the experienced electric field E_x (black curve) and the γ factor (red curve) for AES electrons. The solid curves are for $n_0 = 0.04n_c$ and the dashed curve for $n_0 = 0.02n_c$. (d) Energy spectra of the trapped electrons at $t = 83T_L$ and $t = 101T_L$. The black curves are 1D results, the red curve is a 2D result, and the green curve is obtained according to Eq. (2) at $t = 101T_L$.

Notice that, due to a longer plasma period $2\pi/\omega_{p0}$ at lower n_0, the injection time for the case $n_0 = 0.02n_c$ is delayed by about $4T_L$ as compared to the case $n_0 = 0.04n_c$.

The trapped electrons retain a peaked energy spectrum, as shown in Fig. 2(d). Since the AES electrons originate directly from the first wake spike behind the laser, one expects that they keep the energy spectrum characteristic of the density spike that existed shortly before injection. The energy distribution of electrons within the spike with velocities $\beta_m - \beta_e \ll 1$ obeys

$$dN/d\gamma \propto (\beta_m/\beta_e)/(\beta_m - \beta_e)\gamma^3, \qquad (2)$$

where $\gamma = (1 - \beta_e^2)^{-1/2}$. Assuming that those electrons within the spike having velocities $\beta_e > \beta_{\rm ph}^{\rm plat}$ all go to the AES and afterward are uniformly accelerated in the wake due to the ultrashort bunch duration, the energy spectrum of AES will remain similar to Eq. (2) except for a shift along the γ axis. Then, γ and β_e in Eq. (2) will be replaced by $\gamma - \mathcal{E}$ and $\sqrt{1 - (\gamma - \mathcal{E})^{-2}}$, respectively, where $\mathcal{E} = |E_x|\Delta t$ represents the energy gain normalized by $m_e c^2$, $|E_x|$ is the accelerating electric field normalized by $m_e \omega_L c/e$, Δt is the accelerating time normalized by $1/\omega_L$, and m_e and $-e$ are the electron mass and charge, respectively. The spectrum obtained from Eq. (2) is shown in Fig. 2(d) for the AES accelerated up to $t = 101T_L$, where $\beta_m = 0.98$ is obtained from simulation. Agreement with the simulated

spectrum at the high-energy end is obtained, indicating that the AES stems from the high-energy part of the density spike, while the low-energy electrons arise from continuous injection during further propagation.

In order to estimate the charge, we assume that a wake density spike exists just before injection with β_m larger than $\beta_{\rm ph}^{\rm plat}$. The AES charge Q can then be calculated by integrating over the spike electrons with $\beta_e > \beta_{\rm ph}^{\rm plat}$. The solution for nonlinear plasma oscillations [10] gives $Q \propto n_0 \beta_m^{1/2} \gamma_m^{3/2} (\beta_m - \beta_{\rm ph}^{\rm plat})^{1/2}$ with $\gamma_m = (1 - \beta_m^2)^{-1/2}$, which is substantially less than the total number of electrons within the spike. This scaling indicates that Q increases with n_0 and a_0 because larger a_0 means higher β_m and lower $\beta_{\rm ph}^{\rm plat}$ [19]. Figure 3(a) verifies such a correlation through a series of simulations in which the parameter a_0 was scanned for two different plateau densities. It is seen that a threshold for the laser amplitude $a_{\rm th}$ exists, below which few electrons get trapped. Clearly, this threshold refers to the point at which $\beta_m = \beta_{\rm ph}^{\rm plat}$. Also, it shows that Q saturates for sufficiently high a_0, referring to the ultrarelativistic limit $\beta_{\rm ph}^{\rm plat} = \beta_{\rm ph}^{\rm lim}$. By scanning $a_{\rm th}$ at various n_0, we show that this scheme works over a wide parameter range, as presented in Fig. 3(b). In this sense, tunable AES generation is possible by adjusting experimental conditions. Generally, larger AES charge can be achieved at higher plasma density, requiring lower driver intensity.

An important question is still to determine the laser spot size that is needed in a realistic case. In the bubble regime [23] with a tightly focused spot given by $\omega_{p0}\sigma/c = 2\sqrt{a_0}$ [18], nearly complete blowout occurs due to the strong transverse ponderomotive force of the laser pulse. Here, in order to retain the quasi-1D regime of the wakefield, it is necessary to adopt a spot size larger than the value given above. As shown later, the relatively broad spot also leads to transverse uniformity of AES, and no significant laser filamentation is observed. We conducted 2D PIC simulations of the proposed scheme with the OSIRIS code [24]. The longitudinal laser-target profiles are identical with the above 1D runs. A Gaussian radial shape $\exp(-r^2/\sigma^2)$ for the laser amplitude with $\sigma = 20\lambda_L$ is employed to ensure
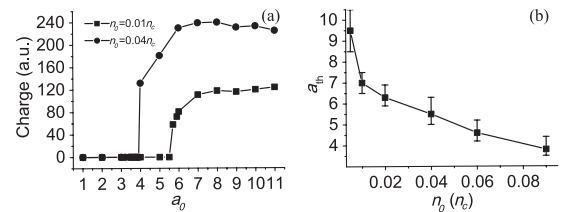

FIG. 3. (a) Charge carried by the AES versus laser amplitude a_0. In the case of $n_0 = 0.04n_c$, the laser-target parameters are $L_1 = 45\lambda_L$ and $\tau_L = 10T_L$, while for $n_0 = 0.01n_c$ they are $L_1 = 80\lambda_L$ and $\tau_L = 14T_L$. (b) Threshold laser amplitude $a_{\rm th}$ versus the plateau density n_0.

the quasi-1D wake. A moving window of $30\lambda_L \times 100\lambda_L$ is used with a 4800×5000 grid. Despite a significant reduction of resolution in these 2D runs, they well reproduce the basic features of AES generation in 1D simulations.

Figures 4(a) and 4(b) show snapshots of the electron density shortly before and after the UPT. A dense sheet with a duration of tens of attoseconds gets trapped near $x = 65\lambda_L$. The AES curvature is essentially a quasi-1D feature arising from the radially nonuniform relativistic correction to the wake period [10,25,26]; i.e., each transverse slice can be derived from a corresponding 1D simulation. Figure 4(c) further shows the AES profile during subsequent acceleration. Its energy spectrum, presented in Fig. 2(d) at $t = 83T_L$, shows a monoenergetic peak with an energy spread less than 0.4 MeV. The AES carries more than 0.5 nC within a diameter of $10\lambda_L$. Its normalized transverse emittance is kept at $\epsilon_\perp < 10$ mm mrad during a short propagation with an average bunch brightness in the order of 10^{18} A/(m rad)^2.

Because of the relatively broad spot, the transverse laser ponderomotive force is very weak. This is clearly shown in Fig. 4(d), where three groups of particle tracks can be distinguished according to their behaviors. For group A, away from the center axis, the electrons simply execute linear local oscillations. The group B electrons, located closer to the center, undergo oscillations with larger amplitude and may be randomly self-injected into the trailing buckets. A synchronized injection after a single wake period, similar to Fig. 2(c), occurs for electrons in group C located near the center, where the laser amplitude exceeds a_{th}. Clearly, these are the electrons forming the AES. From this, one can deduce the AES radius as $R = \sigma\sqrt{\ln(a_0/a_{th})}$. With the present parameters, R amounts to about $13\lambda_L$, which shows good agreement with Fig. 4(c). Note that the breaking of the trailing buckets also occurs at their transitions to the plateau. However, these injected bunches are found to be much weaker and distorted due to complex nonlinear effects such as transverse wave breaking [27]. Only the leading sheet from the first bucket has the superior properties and will dominate all the noisy rest trailing the first clean electron pulse [see the inset in Fig. 4(e)].

Figure 4(e) further illustrates the effect of laser spot size on the energy spectrum of AES. Peaked spectra have been obtained for large spot radii. While, for a spot radius comparable to (or smaller than) the wake wavelength, i.e., $\sigma = 10\lambda_L$, the electron dynamics is no longer quasi-1D [23], and, shortly after transition, transverse wave breaking [27] and self-injection occur, causing a much broader energy distribution. The AES lifetime is limited by the transverse motion of electrons, which is governed by the focusing fields that result from the curvature of wave fronts. This corresponds to several tens of laser periods or 100 femtoseconds in the above simulations. Importantly, attributed to the nonlinear correction to β_{gr}, the transition

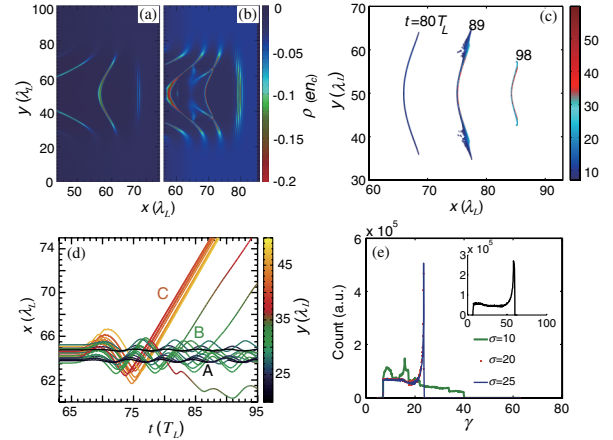FIG. 4 (color online).   Results of 2D PIC simulation. Snapshots (a) and (b) show the electron density at $t = 71T_L$ and $t = 83T_L$, respectively. (c) Snapshots of the trapped electrons (colored according to $\gamma - 1$) during acceleration. (d) Particle-tracking plot. It is obtained by first tracking back AES electrons to find their initial x range and then tracking a random sample of 24 electrons within this x range. ($y = 50\lambda_L$ corresponds to the center axis.) (e) Energy spectra of the trapped electrons for different spot radii at $t = 83T_L$ while keeping the other parameters fixed. The inset shows a spectrum at $t = 98T_L$ for $\sigma = 20\lambda_L$.

of β_{ph} from above to below unity does not exactly occur where the plateau begins [see Fig. 1(b)]. This implies that a density ramp of strictly linear slope is not necessary. Actually, we have tested smoother ramped profiles, e.g., parabolic or $\tanh(x)$, and few differences from the above were found.

In conclusion, an underdense plasma target with a density up ramp attached in the front and a sufficiently intense laser can lead to localized injection of a dense electron bunch at the transition to a following density plateau. A broad laser spot greater than the wake wavelength leads to wakefield excitation in the quasi-1D regime. PIC simulations show that a boosted electron sheet can be produced carrying unique characteristics, such as density well above n_c, attosecond duration, high charge ($\sim$ nC), transverse uniformity, and even small absolute energy spread. This scenario works over a wide parameter range. The AES has a sufficient lifetime for envisioned applications, particularly for coherent Thomson scattering [4,6]. It may also serve as a synchronized injection source for staged laser wakefield accelerators with applications in next generation accelerators [25,28] and light sources due to its high charge and brightness.

*zmsheng@sjtu.edu.cn

[1] G. A. Mourou, T. Tajima, and S. V. Bulanov, Rev. Mod. Phys. **78**, 309 (2006).

[2] E. Esarey, C. Schroeder, and W. Leemans, Rev. Mod. Phys. **81**, 1229 (2009).

[3] J. Faure, Y. Glinec, A. Pukhov, S. Kiselev, S. Gordienko, E. Lefebvre, J.-P. Rousseau, F. Burgy, and V. Malka, Nature (London) **431**, 541 (2004); C. Geddes, Cs. Toth, J. van Tilborg, E. Esarey, C. B. Schroeder, D. Bruhwiler, C. Nieter, J. Cary, and W. P. Leemans, Nature (London) **431**, 538 (2004); S. Mangles *et al.*, Nature (London) **431**, 535 (2004); W. Leemans, B. Nagler, A. J. Gonsalves, Cs. Tóth, K. Nakamura, C. G. R. Geddes, E. Esarey, C. B. Schroeder, and S. M. Hooker, Nat. Phys. **2**, 696 (2006).

[4] H. C. Wu and J. Meyer-ter-Vehn, Eur. Phys. J. D **55**, 443 (2009).

[5] G. V. Stupakov and M. S. Zolotorev, Phys. Rev. Lett. **86**, 5274 (2001).

[6] B. Rau, T. Tajima, and H. Hojo, Phys. Rev. Lett. **78**, 3310 (1997); V. V. Kulagin, V. A. Cherepenin, M. S. Hur, and H. Suk, Phys. Rev. Lett. **99**, 124801 (2007); J. Meyer-ter-Vehn and H. C. Wu, Eur. Phys. J. D **55**, 433 (2009); H. C. Wu, J. Meyer-ter-Vehn, J. Fernandez, and B. M. Hegelich, Phys. Rev. Lett. **104**, 234801 (2010).

[7] N. Naumova, I. Sokolov, J. Nees, A. Maksimchuk, V. Yanovsky, and G. Mourou, Phys. Rev. Lett. **93**, 195003 (2004); Y. Y. Ma, Z.-M. Sheng, Y.-T. Li, W.-W. Chang, X.-H. Yuan, M. Chen, H.-C. Wu, J. Zheng, and J. Zhang, Phys. Plasmas **13**, 110702 (2006).

[8] T. V. Liseykina, S. Pirner, and D. Bauer, Phys. Rev. Lett. **104**, 095002 (2010).

[9] I. Y. Dodin and N. J. Fisch, Phys. Rev. Lett. **98**, 234801 (2007).

[10] A. Akhiezer and R. Polovin, Sov. Phys. JETP **3**, 696 (1956).

[11] C. D. Decker, W. B. Mori, K.-C. Tzeng, and T. Katsouleas, Phys. Plasmas **3**, 2047 (1996); S. V. Bulanov, T. Esirkepov, and T. Tajima, Phys. Rev. Lett. **91**, 085001 (2003); M. Kando *et al.*, Phys. Rev. Lett. **99**, 135001 (2007).

[12] T. Katsouleas and W. B. Mori, Phys. Rev. Lett. **61**, 90 (1988); Z. M. Sheng and J. Meyer-ter-Vehn, Phys. Plasmas **4**, 493 (1997).

[13] E. Esarey, R. F. Hubbard, W. P. Leemans, A. Ting, and P. Sprangle, Phys. Rev. Lett. **79**, 2682 (1997); J. Faure, C. Rechatin, A. Norlin, A. Lifschitz, Y. Glinec, and V. Malka, Nature (London) **444**, 737 (2006); P. Zhang, N. Saleh, S. Chen, Z. M. Sheng, and D. Umstadter, Phys. Rev. Lett. **91**, 225001 (2003).

[14] M. Chen, Z.-M. Sheng, Y.-Y. Ma, and J. Zhang, J. Appl. Phys. **99**, 056109 (2006); A. Pak, K. A. Marsh, S. F. Martins, W. Lu, W. B. Mori, and C. Joshi, Phys. Rev. Lett. **104**, 025003 (2010); C. McGuffey *et al.*, Phys. Rev. Lett. **104**, 025004 (2010); M. Chen, E. Esarey, C. B. Schroeder, C. G. R. Geddes, and W. P. Leemans, Phys. Plasmas **19**, 033101 (2012).

[15] S. Bulanov, N. Naumova, F. Pegoraro, and J. Sakai, Phys. Rev. E **58**, R5257 (1998); C. G. R. Geddes, K. Nakamura, G. Plateau, Cs. Toth, E. Cormier-Michel, E. Esarey, C. Schroeder, J. Cary, and W. Leemans, Phys. Rev. Lett. **100**, 215004 (2008); K. Schmid, A. Buck, C. M. S. Sears, J. M. Mikhailova, R. Tautz, D. Herrmann, M. Geissler, F. Krausz, and L. Veisz, Phys. Rev. ST Accel. Beams **13**, 091301 (2010).

[16] J. Vieira, S. F. Martins, V. B. Pathak, R. A. Fonseca, W. B. Mori, and L. O. Silva, Phys. Rev. Lett. **106**, 225001 (2011).

[17] T. Katsouleas, Phys. Rev. A **33**, 2056 (1986).

[18] W. Lu, M. Tzoufras, C. Joshi, F. Tsung, W. Mori, J. Vieira, R. Fonseca, and L. Silva, Phys. Rev. ST Accel. Beams **10**, 061301 (2007).

[19] C. B. Schroeder, C. Benedetti, E. Esarey, and W. P. Leemans, Phys. Rev. Lett. **106**, 135002 (2011).

[20] Z. M. Sheng, Y. Sentoku, K. Mima, J. Zhang, W. Yu, and J. Meyer-ter-Vehn, Phys. Rev. Lett. **85**, 5340 (2000); M. Chen *et al.*, Chin. J. Comput. Phys. **25**, 43 (2008).

[21] S. Bulanov *et al.*, J. Plasma Phys. **16**, 444 (1990).

[22] C.-L. Chang, C.-T. Hsieh, Y.-C. Ho, Y.-S. Chen, J.-Y. Lin, J. Wang, and S.-Y. Chen, Phys. Rev. E **75**, 036402 (2007); M.-W. Lin, Y.-M. Chen, C.-H. Pai, C.-C. Kuo, K.-H. Lee, J. Wang, S.-Y. Chen, and J.-Y. Lin, Phys. Plasmas **13**, 110701 (2006).

[23] A. Pukhov and J. Meyer-ter-Vehn, Appl. Phys. B **74**, 355 (2002); W. Lu, C. Huang, M. Zhou, W. B. Mori, and T. Katsouleas, Phys. Rev. Lett. **96**, 165002 (2006).

[24] R. Fonseca *et al.*, *Proceedings of the Second International Conference on Computational Science—ICCS, Amsterdam, 2002, Lecture*, Notes in Computer Science Vol. 2331 (Springer, Berlin, 2002), p. 342.

[25] S. Y. Kalmykov, L. M. Gorbunov, P. Mora, and G. Shvets, Phys. Plasmas **13**, 113102 (2006).

[26] N. H. Matlis *et al.*, Nat. Phys. **2**, 749 (2006); P. Dong *et al.*, New J. Phys. **12**, 045016 (2010).

[27] S. V. Bulanov, F. Pegoraro, A. M. Pukhov, and A. S. Sakharov, Phys. Rev. Lett. **78**, 4205 (1997).

[28] S. F. Martins, R. A. Fonseca, W. Lu, W. B. Mori, and L. O. Silva, Nat. Phys. **6**, 311 (2010); T. Mehrling, J. Grebenyuk, F. S. Tsung, K. Floettmann, and J. Osterhoff, Phys. Rev. ST Accel. Beams **15**, 111303 (2012).